

# Structure and Dynamics of Water Confined in Imogolite Nanotubes

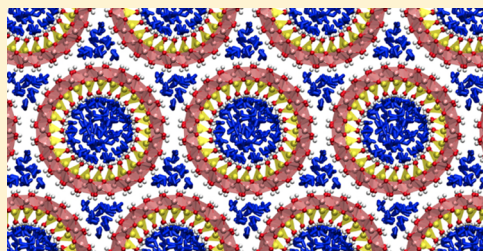
Laura Scalfi,<sup>†</sup> Guillaume Fraux,<sup>‡</sup> Anne Boutin,<sup>\*,†</sup> and François-Xavier Coudert<sup>\*,‡</sup>

<sup>†</sup>PASTEUR, Département de Chimie, École Normale Supérieure, PSL University, Sorbonne Université, CNRS, 75005 Paris, France

<sup>‡</sup>Chimie ParisTech, PSL University, CNRS, Institut de Recherche de Chimie Paris, 75005 Paris, France

## Supporting Information

**ABSTRACT:** We have studied the properties of water adsorbed inside nanotubes of hydrophilic imogolite, an aluminum silicate clay mineral, by means of molecular simulations. We used a classical force field to describe the water and the flexible imogolite nanotube and validated it against the data obtained from first-principles molecular dynamics. With it, we observe a strong structuration of the water confined in the nanotube, with specific adsorption sites and a distribution of hydrogen bond patterns. The combination of number of adsorption sites, their geometry, and the preferential tetrahedral hydrogen bonding pattern of water leads to frustration and disorder. We further characterize the dynamics of the water, as well as the hydrogen bonds formed between water molecules and the nanotube, which is found to be more than 1 order of magnitude longer than water–water hydrogen bonds.



## INTRODUCTION

Imogolite is an aluminum silicate clay mineral, with formula  $\text{Al}_2\text{SiO}_3(\text{OH})_4$ , that was first discovered in volcanic ashes in Japan.<sup>1</sup> It is the only known aluminosilicate material that spontaneously forms inorganic nanotubes, and there exists no planar equivalent material in nature—unlike carbon nanotubes, of which graphene is the planar form. Imogolite nanotubes are monodisperse in diameter and can be readily synthesized with controlled length and diameter, for example, by substituting silicon with germanium.<sup>2</sup> This precise control of the imogolite nanotube dimensions is interesting for applications that rely on one-dimensional pore channels in fields, such as nanofluidic devices, membranes for filtration and separation, desalination, and so forth. Moreover, from a theoretical point of view, its hollow cylindrical topology and tunable size make it a very attractive model to study the properties of fluids under confinement.

Although imogolites have been the subject of several experimental studies, only a few theoretical works have been carried out until now. In particular, there is relatively little data—experimental or computational—on the hydration of these nanotubes, and the behavior of the confined water molecules inside the pore space. Imogolite nanotubes differ markedly from the more common carbon nanotubes in both geometry and chemistry, and the behavior of water inside their pores is still very much open. It is experimentally challenging to address these issues, especially differentiating the water inside the nanotubes from the water outside, and a computational approach through molecular modeling is therefore a natural complement to the published experimental results.

A single imogolite nanotube presents two surfaces, both available for adsorption. The outer surface is composed of a gibbsite-like sheet of aluminum octahedra. The inner surface is formed of silicon tetrahedra with one hydroxyl group pending

and the three other corners of the tetrahedron linked to three aluminum octahedra. Therefore, both surfaces are covered with hydroxyl groups that are expected to have a hydrophilic behavior. On the basis of electrostatic calculations, authors have suggested that the inner surface is strongly hydrophilic, whereas the outer surface might be more hydrophobic.<sup>3,4</sup>

Most of the theoretical studies on imogolite nanotubes focus on the energetics of empty nanotubes. The sharp monodispersity in nanotube diameters has been explained by both quantum chemistry and classical studies that show the strain energy has a minimum for a given nanotube diameter, contrary to carbon nanotubes, where the energetically favorable structure is that of infinite diameter (i.e., the graphene slab<sup>4–7</sup>). Several studies also focused on computing vibrational spectra<sup>5,8,9</sup> and studying the energetics and dynamics of the rolling of the nanotubes themselves.<sup>10–12</sup> Finally, other works have pointed at more complex aspects, such as defects<sup>3</sup> and deformation or hexagonalization of the nanotubes.<sup>5,13,14</sup>

Because adsorption on the outer surface of the nanotubes depends strongly on experimental conditions affecting the bundling of the nanotubes, and therefore the spacing between them, we will focus in the present work on the adsorption and behavior of water confined inside imogolite nanotubes. Moreover, the strong curvature and the limited space inside the nanotube provide for strong confinement effects on which little experimental data is available. We have used a classical force field to describe the water and the flexible imogolite nanotube, which we validate against structural data obtained from first-principles molecular dynamics (MD). From classical grand canonical Monte Carlo (GCMC) and MD simulation, we

Received: April 5, 2018

Revised: May 18, 2018

Published: May 21, 2018

observe a strong structuration of the water confined in the nanotube, with specific adsorption sites, and a statistical distribution of hydrogen bond patterns. The combination of number of adsorption sites, their geometry, and the preferential tetrahedral hydrogen bonding pattern of the water leads to frustration and disorder. We also characterize the dynamics of the water, as well as the hydrogen bonds formed between water molecules and the nanotube.

## ■ SYSTEMS

**Imogolite Structure.** Imogolites are aluminum silicate clay minerals with the chemical formula  $(\text{OH})_3\text{Al}_2\text{O}_5\text{SiOH}$ . Their structure was first described by Cradwick et al.<sup>15</sup> from electron diffraction measurements as a cylindrical assembly of silicon tetrahedra and aluminum octahedra (see Figure 1). This sheet

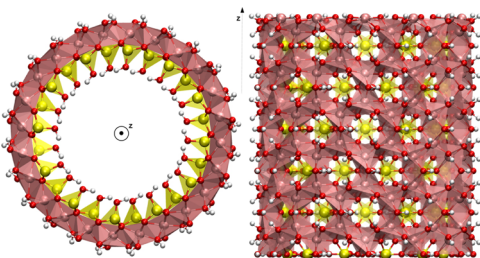


**Figure 1.** Imogolite nanotube ( $n = 12$ ) with three unit cells along the tube axis  $z$ . Color code: aluminum (pink), silicon (yellow), oxygen (red), and hydrogen (white). Note the hydrogen bonds between silanol groups on the inner surface (left panel).

spontaneously folds into a nanotube because of bond length mismatch and the formation of hydrogen bonds.<sup>10,11</sup> The imogolite nanotubes are characterized using the same nomenclature as carbon nanotubes. Both natural and synthetic imogolite nanotubes exhibit a zig-zag folding, with a variable number  $n$  of  $(\text{OH})_3\text{Al}_2\text{O}_5\text{SiOH}$  units (called gibbsite units) along the nanotube circumference. The cylindrical unit cell then contains  $2n$  gibbsite units. Natural imogolite is a nanotube with size  $n = 12$ , whereas depending on the details of the synthesis conditions, synthetic imogolites correspond to values of  $n$  typically between 12 and 14 and sometimes larger.

To produce imogolite nanotube models, we started from the structure of Cradwick et al.<sup>15</sup> for a  $n = 10$  nanotube with  $C_{2n}$  symmetry. We formed a flat gibbsite-like sheet by unfolding the nanotube and adding hydrogen atoms (not present on the electron diffraction data). We relaxed the slab geometry and unit cell with density functional theory (DFT, see computational details in the next section) in the  $C_m$  space group. From this relaxed planar structure, we rolled back a nanotube of size  $n = 12$ . Using the Bilbao Crystallographic Server,<sup>16</sup> we identified the space group of the nanotube to be  $P4/m$ . We relaxed the nanotube structure and cell parameters with periodic DFT calculations, using a large inter-nanotube spacing (60 Å), so that there are no interactions between nanotubes. We show in Figure 1 the two views from the top and side of the  $n = 12$  nanotube with three unit cells along the  $z$ -axis.

The internal surface of an imogolite nanotube can be described as a periodic sequence of silicon rings along the nanotube axis. Two adjacent rings are rotated of  $\pi/n$ . When dry, silanol groups within a ring form hydrogen bonds so that all of the hydroxyl groups are in a plane normal to the nanotube axis, as shown in Figure 1. The internal diameter, computed

between internal oxygen (noted  $O_{\text{int}}$ ), is 12.8 Å, and the external diameter, computed between external oxygen (noted  $O_{\text{ext}}$ ), is approximately 22 Å. Konduri et al.<sup>17</sup> highlighted that as a consequence, the inner pore is not smooth and uniform as for the carbon nanotube, but the pore is rugged: narrower where there are silanol groups and larger between these silicon rings. One can picture the internal cavity as a hollow cylinder with equally spaced circular furrows in the circumference.

**Nanotubes Packing.** Imogolite nanotubes can have a length from 10 nm up to a few micrometers, and experiments show that they tend to pack into bundles when dry. The periodic pattern seems to be a monoclinic assembly<sup>18,19</sup> with  $\beta \approx 78^\circ$ . Given our focus on adsorption inside the nanotubes, following other theoretical studies, we chose to represent the nanotubes in a hexagonal packing that is close to the monoclinic one.<sup>8,17,20</sup> Lattice constants are chosen to ensure close contact (but no overlap) between neighboring nanotubes, at  $a = b = 24.2$  Å. This choice is consistent with the experiments and other theoretical studies. Along the tube axis, we studied supercells with lattice parameters  $c = n \times 8.486$  Å, where  $n = 1, 3$ , or  $5$  (where the value of 8.486 Å was determined by geometry optimization with variable cell).

**Simulation Methods.** We performed simulations at two different levels of theory: at the quantum chemistry level, we performed DFT calculations for both energy minimization as well as first principles MD. We also used classical force-field-based simulations, for both classical MD and Monte Carlo simulations. We used the open source cfiles tool (<https://github.com/chemfiles/cfiles>) for trajectory analysis: angles distribution, density maps and hydrogen bonding patterns. Representative input files for the molecular simulations are available online in our data repository at <https://github.com/fcoudert/citable-data>.

**DFT Calculations.** Energy minimization of the nanotubes and slabs were performed with DFT calculations with periodic boundary conditions and the use of symmetry to reduce computational cost. We used these calculations with the CRYSTAL14<sup>21</sup> software package. The exchange–correlation functional used was the solid-adapted generalized gradient approximation PBEsol, and the basis set for all atoms (Si, Al, O, H) was double- $\zeta$  valence polarized.

We also performed DFT-based MD simulations, also known as first principles or *ab initio* MD, as a way to generate reference data for comparison and validation of classical force fields. These simulations were run with CP2K.<sup>22</sup> Temperature was kept constant at 300 K with a canonical sampling through velocity rescaling thermostat,<sup>23</sup> with a time constant of 200 fs. The timestep was 0.5 fs, and the system was deuterated for computational convenience. After 5 ps of equilibration, production trajectories were accumulated for 30 ps.

**Classical Simulations.** Although DFT is a good model to extract the structure and short-time dynamics of the system, simulations longer than a few tens of picoseconds are not readily accessible. This is why we used classical simulations based on a force field approximation of the intra- and intermolecular interactions, to study the structure and dynamics of water in imogolites at larger time scales. We ran MD simulations in the canonical ( $N, V, T$ ) ensemble with the LAMMPS code,<sup>24</sup> using a timestep of 0.5 fs. After 100 ps of equilibration, we collected trajectories from 200 ps to 50 ns, depending on the properties studied in each case.

We also performed a series of GCMC simulations with a fixed chemical potential, volume, and temperature ( $\mu, V, T$ ) to

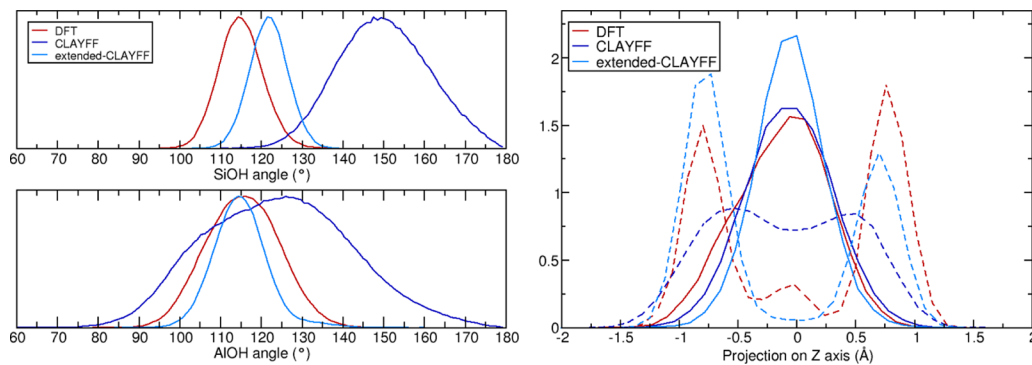


**Figure 2.** Left: Angle distributions for Si–O<sub>int</sub>–H<sub>int</sub> angles (top) and Al–O<sub>ext</sub>–H<sub>ext</sub> angles (bottom) for DFT (red line), CLAYFF (dark blue line) and extended-CLAYFF (sky blue line) simulations. Right: Density of the internal hydrogen atoms, H<sub>int</sub>, along the nanotube axis z for an empty nanotube (solid lines) and a fully hydrated nanotube (dashed lines). Data from DFT are shown in red, data from CLAYFF in dark blue, and from extended-CLAYFF in sky blue.

simulate the behavior of the system in equilibrium with a reservoir at a given pressure linked to the chemical potential. In the gas phase, water was considered to be an ideal gas, and the chemical potential is then easily linked to the gas pressure.<sup>25</sup> Series of GCMC simulations were used to compute adsorption isotherms, with the water vapor pressure going from 2 to 3600 Pa.

To describe the interactions of the nanotube, we relied on the CLAYFF force field,<sup>26</sup> which has been extensively used in the literature.<sup>12,17,20</sup> Water was described in the flexible single-point charge (fSPC) model,<sup>27</sup> which is naturally suited for coupling with CLAYFF. CLAYFF is a general force field developed to model clay minerals that have the same chemical nature of the imogolite. It relies almost exclusively on nonbonded interactions, where interatomic potentials are the sum of electrostatic (Coulombic) and dispersive–repulsive (Lennard-Jones 12-6) interactions. In addition to these nonbonding interactions, CLAYFF includes a harmonic bond term for hydroxyl bonds (O–H stretching). Moreover, CLAYFF can be extended by the use of an additional M–O–H harmonic bending potential, although this term is not generally used and not necessary to reproduce clay structures. We call the resulting force field “extended CLAYFF”, and in this work we have used both CLAYFF and extended CLAYFF. We show later that the M–O–H bending potential is crucial for simulating imogolite nanotubes, especially for adsorption properties.

## RESULTS AND DISCUSSION

**Validation of the Force Field.** The CLAYFF force field has been used in the literature for classical molecular simulations of imogolite nanotubes,<sup>12,17,20</sup> owing to the similarities between clays and imogolite. Here, we set out to check its validity in the description of both empty imogolite nanotubes as well as water-filled tubes. As a reference, we compared it to trajectories obtained from first-principles MD, where the evaluation of interatomic forces is carried out at the DFT level. We found that the structure of the nanotube itself is relatively rigid and dictated by equilibrium Si–O and Al–O bond lengths, so that the skeleton (aluminum Al, silicon Si, and bridging oxygen O<sub>br</sub>) is well-reproduced with the CLAYFF potential (in both variants).

Second, we focus on the description of the inner and outer surface groups. We plot in Figure 2 the calculated distributions of Si–O<sub>int</sub>–H<sub>int</sub> angles for silanol groups inside the tube and

Al–O<sub>ext</sub>–H<sub>ext</sub> angles for AlOH groups on the outer surface. There are clear discrepancies between CLAYFF results and reference first principles data: average M–O–H angles are much larger and their distribution broader. For CLAYFF, angles go all the way up to 180° and, for AlOH, down below 90°; this contrasts with the clearly Gaussian distributions obtained by DFT and centered at 115° and 117° for SiOH and AlOH, respectively.

In contrast, augmenting the CLAYFF force field with the additional M–O–H bending term (the “extended CLAYFF”) leads to a clear improvement of the imogolite description. The distributions of both SiOH and AlOH angles are closer to those obtained from the first-principles MD, although the match is not perfect—as could be expected for a generic force field without ad hoc reparameterization. The average value of the SiOH angle with extended CLAYFF is 122°, which is 7° larger than the reference data. The same is true of the outer AlOH groups.

These discrepancies in imogolite structure strongly affect water–imogolite interactions, and from here water adsorption, structure and dynamics. To further assess the necessity of using the extended CLAYFF instead of CLAYFF, we performed simulations of fully hydrated nanotubes and compared them against data from first-principles MD. On the right panel of Figure 2, we show the density profiles along the nanotube axis z for the internal hydrogens. First, we observe that in the empty nanotube, the density distributions are all around z = 0 (the plane in which are located the silicon atoms). This allows hydrogen bonding with other silanol groups in the same z = 0 plane. Second, upon hydration, there is a clear move of the SiOH hydrogen atoms toward symmetric positions at  $\pm 0.75$  Å because of hydrogen bonding with the water molecules—a detailed analysis of this hydrated structure will be given below. This change in the H localization, which we observe in the first-principles MD, is well-reproduced by the extended CLAYFF force field. However, it is markedly different in regular CLAYFF, where we see a unique broad population with two bumps. Thus, the distribution of internal hydrogen atoms, fundamental for adsorption studies and the description of hydrated imogolites, is best described by the extended CLAYFF model. This aspect has been recently studied by Pouvreau et al.<sup>28</sup> that similarly showed the necessity of an M–O–H bending term to properly describe basal and edge surfaces of gibbsite and brucite. From here on, we will use exclusively the extended CLAYFF force field.

**Water Adsorption.** To characterize water adsorption in the gas phase and obtain physically meaningful water uptake values, we performed GCMC simulations for water pressure between 2 and 3600 Pa. Full details of the simulations, performed with two different water models (SPC and TIP4P05), are presented in the Supporting Information, as well as isotherms. For computational reasons, rigid water models were preferred in the GCMC calculations. We observe (Figure S1) that the imogolite nanotube is hydrophilic, that is, the filling occurs at a pressure below the bulk saturation pressure. This is in agreement with the affinity of water for silanol-rich surfaces or zeolites with many silanol defects.<sup>29</sup> The value of the pore-filling pressure varies strongly with the nature of the model chosen for the description of the water, and the movement allowed for the silanol groups—consistent with the findings of Zang et al.<sup>20</sup> We find transition pressures of 0.1 kPa for TIP4P05 and 1 kPa for the SPC water model. The order of magnitude of those values are within the range of experimental data, for example, the gravimetric study of Konduri et al.,<sup>17</sup> which features a smooth isotherm with water uptake in the same range (0.1–1 kPa; see Figure S1).

In contrast to the adsorption pressure model dependence, there is an excellent agreement between the various models on the saturation uptake of water once the pore is filled, that is, on the density of the water adsorbed inside the imogolite nanotube. Uptake is found to be 10% by weight after the transition, both for the SPC and TIP4P05 water models. We thus derived from the GCMC calculations an initial configuration for the simulation of the fully filled imogolite nanotube, from the plateau of the SPC adsorption isotherm. This initial configuration contains three nanotubes ( $n = 12$ ) unit cells along the  $z$ -axis, 98 water molecules inside the nanotubes and 18 water molecules outside. It is represented in Figure 3. We used this fully hydrated tube as a starting configuration for classical MD simulation, with the extended CLAYFF force field and fSPC water model.

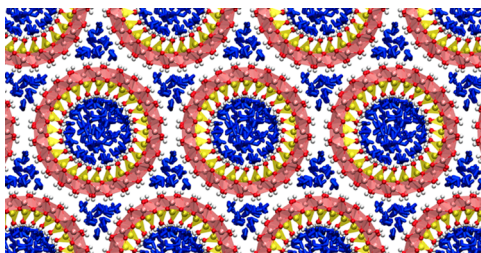


**Figure 3.** Fully hydrated imogolite nanotube ( $n = 12$ ) with hexagonal packing. Water molecules are represented as blue sticks.

**Structure of Confined Water.** From the analysis of the MD trajectories of the fully hydrated imogolite, we computed density profiles of all-atom types (water  $O_w$  and  $H_w$ ; silanol groups Si,  $O_{int}$ , and  $H_{int}$ ). They are plotted in Figure 4 in the  $xy$  plane, that is, as if viewed “from the top” of the (infinite) nanotube. From the water oxygen distribution  $O_w$ , it is clear that there are two different populations of water molecules: strongly structured water adsorbed next to the inner surface (a first hydration layer, at distances between 4.5 and 5.8 Å from the nanotube’s center) and more disordered water filling up the center of the nanotube. This is also clearly visible in the cylindrical distribution functions (Figure S2), where we see that the two populations are not completely separate, that is, the

density does not fall to zero in-between. Furthermore, we see a slight deviation of the nanotube from a purely circular form: the position of the Si atoms shows a slightly hexagonal deformation because of the symmetry of the packing of nanotubes in bundles.<sup>13</sup> This deformation is only very small, with Si displacements of 0.1–0.2 Å at most because of the rigid nature of the imogolite nanotube, especially with such a small diameter. This deformation is both linked to the hexagonal packing and the adsorption stress exerted by the water molecules—as shown previously, for water/quartz interfaces,<sup>30</sup> and more generally for adsorbates in “soft” porous materials.<sup>31,32</sup> In the case of imogolite, the stress exerted is counterbalanced by the relative stiffness of the nanotube, although the extent and details of the deformation depend on the packing of the nanotubes. For example, Creton et al.<sup>14</sup> used a larger distance between the nanotubes and observed a transition between an ellipsoid shape to a more cylindrical shape, when increasing water density.

To better understand the structuration of the first adsorbed layer, we plot in Figure 5 the same densities, but this time as a function of cylindrical coordinates  $z$  and  $\rho$ , where  $\rho$  is the distance to the central axis of the nanotube. There, the strongly preferential location for the confined water oxygen atoms becomes clear: the water molecules sit in the wider furrows, situated in between two rings of silanol groups (SiOH rings are situated every 4.25 Å along the  $z$ -axis and are depicted in Figure 5 by dotted lines). This preferential localization of the adsorbed water contrasts sharply with that of water inside carbon nanotubes, whose internal surface is smoother. It was, however, demonstrated in other nanopores of small dimensions with “dangling” hydroxyl groups accessible to the water for hydrogen bonding.<sup>33</sup>

These molecules are strongly hydrogen-bonded to the silanol groups, as indicated by the well-defined positions for  $H_{int}$  atoms, which are rearranged compared to their relaxed position. Indeed, in the dry imogolite nanotube, the most stable position for the internal hydrogens is in the silanol ring plane ( $z = 0$ ), where they are pointing toward a neighboring  $O_{int}$  atom. This conformation allows the formation of a relatively weak hydrogen bond because the  $O_{int}–H_{int}…O_{int}$  distance is large. In the hydrated tube, the hydrogen atoms’ most common position is shifted out of that silanol ring plane (see Figure 5). This is reflected by a change in the  $O_{br}–Si–O_{int}–H_{int}$  dihedral angle (see Figure S3), which goes from 0° to 60°; where  $O_{br}$  is the oxygen atom bridging the aluminum to the silicon.

We thus propose the following model to better visualize and understand the structure of the adsorbed water. We model the inner surface of the nanotube as a periodic sequence of triangles, where each silanol group SiOH is a vertex. The Si–Si and O–O radial distribution functions show two first neighbor peaks at 4.2 and 4.7 Å for silicon and at 3.3 and 4.6 Å for internal oxygen. This means that the triangles are isosceles with two angles of 66.5° and one angle of 47°. This pattern is depicted in Figure 6. Above the center of each triangle is a potential water adsorption site. However, analysis of the sites show that no neighboring sites in the same  $xy$  plane can be occupied at the same time because of short-distance intermolecular repulsion of water molecules, so that at most half of the adsorption sites are occupied in the filled tube. Then, each of the hydrogen atoms of the SiOH groups that form the vertices of a triangle will point toward one of the three occupied neighboring adsorption sites.

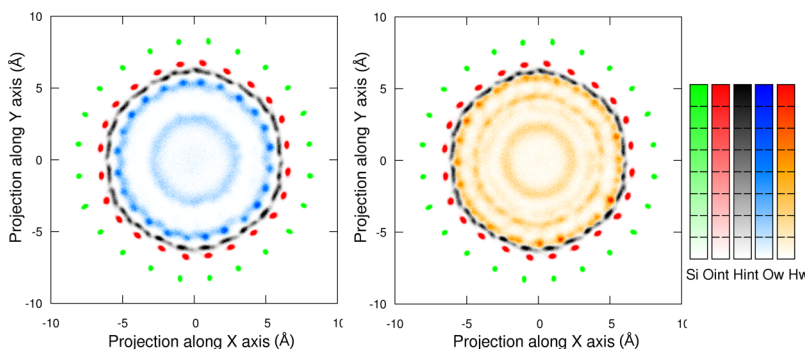


**Figure 4.** Two-dimensional density profiles in the  $xy$  plane for atoms from the silanols groups (Si,  $O_{int}$ , and  $H_{int}$ ) and water molecules ( $O_w$  on the left pane,  $H_w$  on the right pane).

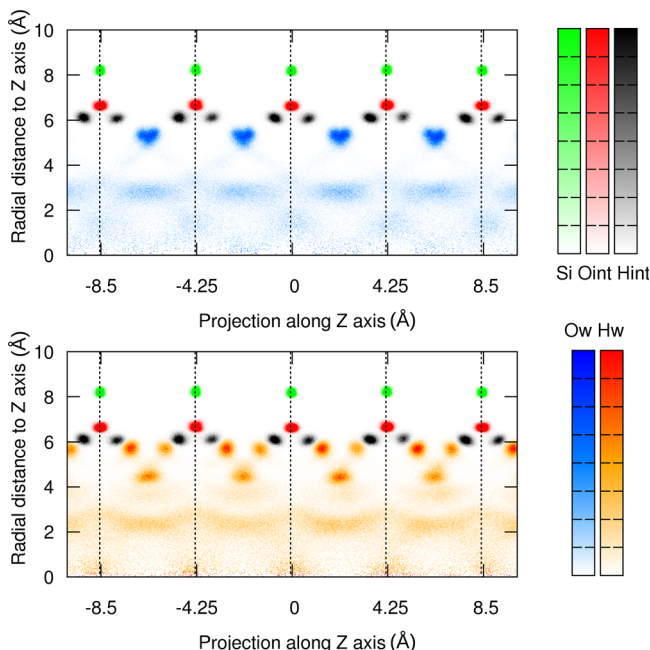


**Figure 5.** Two-dimensional density profiles (the radial dimension vs the projection along the  $z$ -axis) for surface atoms (Si,  $O_{int}$ , and  $H_{int}$ ) and water atoms ( $O_w$  and  $H_w$ ). Silicon rings are indicated by dashed lines. Density profiles are normalized so that for each atom type, the highest value is set to 1.0 (full color intensity).

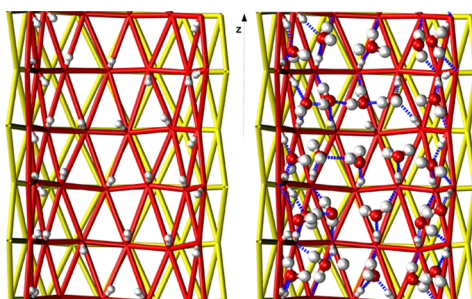


**Figure 6.** Illustration of the model on the  $n = 12$  nanotube (only half of the nanotube is shown). The triangular adsorption sites are highlighted by drawing yellow triangles between silicon atoms and red triangles between oxygen atoms. In the right panel, water molecules within the first adsorption layer are drawn, and hydrogen bonds are depicted in dotted blue sticks.

A final visualization can be obtained by a density plot of O and H atoms, where the density is mapped against  $z$  and a

circular coordinate, as if a slice of the nanotube had been “cut and unrolled”. These densities are presented in Figure 7. Red dotted lines show the SiOH rings, whereas orange dotted lines show the triangular mesh described above. The adsorption sites on top of each triangle are clearly visible. We further see that there is a strong anisotropy of the system, where there is possible circular movement of the water molecules in-between

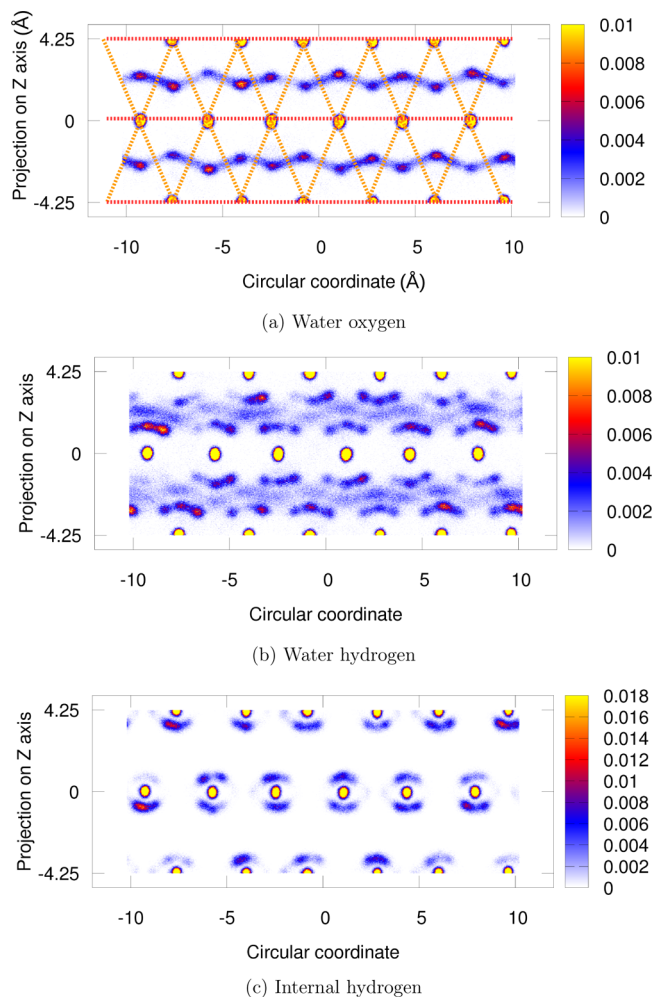


**Figure 7.** Density profiles on the flattened hydrated nanotube planes for water oxygen, water hydrogen, and internal hydrogen. The circular coordinate corresponds to a curvilinear abscissa that draws a circle of radius  $R = 6.5 \text{ \AA}$  centered on the axis  $z$ . On all of the graphs, internal oxygen appear as yellow dots.

sites in the same  $z$  plane, whereas there is no observed density crossing the silanol rings, as already observed by Creton et al.<sup>14</sup> This shows that there is surface diffusion of water molecules, but only in the  $xy$  plane.

**Hydrogen Bond Patterns.** The localization of the first layer of adsorbed water on the inner surface of the imogolite nanotube and the strong hydrogen bonds that are created with the tube's silanol groups make the first layer of water strongly ordered. We can see in Figure 5 (bottom panel) that this includes rotational ordering of the water molecules, with three marked preferential positions for their hydrogen atoms at room temperature. Two of those, equivalent by symmetry, correspond to the formation of a hydrogen bond, donated by the water molecule to the silanol group (acting as acceptor). The third position corresponds to a hydrogen atom "dangling" toward the inside of the nanotube. Because the water molecules have two hydrogen atoms that can occupy these positions, there are three possible geometries, summarized in Figure 8: a water molecule can be donating two hydrogen bonds (case A); accepting one and donating one (case B); or accepting two hydrogen bonds from neighboring silanol groups (case C).

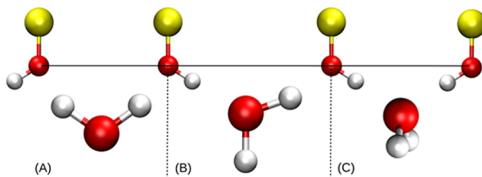


**Figure 8.** Three possible geometries of water adsorbed in the first layer of the imogolite inner surface.

In this section, we quantified the hydrogen-bond network and dynamics with a set of geometric criteria that are commonly used in the literature for hydrogen bonds in water. We consider a hydrogen bond D–H $\cdots$ A to be present between donor atom D and acceptor atom A if, and only if, the D $\cdots$ A distance is less than 3.5 Å and the H $\Delta$ A angle is less than 30°.<sup>34</sup> We performed the hydrogen bond analysis on the hydrated and empty nanotubes and differentiated the types of hydrogen bonds according to the donor and acceptor groups. Water hydroxyls and silanols can both be donor and acceptor.

The average number of hydrogen bonds formed during the trajectory is presented in Table 1. The change in silanol–silanol

**Table 1. Average Number of Hydrogen Bonds ( $\pm$  the Standard Deviation) for Given Donor–Acceptor Pairs along a 1 ns Trajectory of Empty and Hydrated Nanotubes<sup>a</sup>**

donor	acceptor	empty nanotube	hydrated nanotube
silanol	silanol	$35.4 \pm 2.3$	$2.0 \pm 1.3$
water	silanol	$69.0 \pm 2.1$	
silanol	water	$68.7 \pm 1.7$	
water	water	$112.4 \pm 3.7$	

<sup>a</sup>Total number of silanol groups: 72; total number of water molecules: 98.

hydrogen bonding confirms the structural change upon adsorption: when the nanotube is empty, approximately half of the silanol groups are linked by a hydrogen bond within silicon rings (as detected per our rather strict criteria). When hydrated, only 2% form a hydrogen bond with another silanol group. Regarding the hydrogen bonds between a water

molecule and the surface, 94% of the silanol groups donate a hydrogen bond to a water molecule and each silanol group receives on average 0.96 hydrogen bonds from water. Because a silanol group can donate only one hydrogen bond and can receive one or two hydrogen bonds, the bonding possibilities of the surface are extensively used. Within the nanotube, on average, 57% of water molecules receive or donate at least one hydrogen bond from or to a silanol group, that is, are in the first adsorbed layer.

To further characterize the local hydrogen bond network, we considered all four singular hydrogen bonding behaviors possible for a single water molecule: donating to a silanol or a water molecule or accepting from either. Each of these singular behaviors can appear zero, once, or twice. The patterns that represent more than 5% of the occurrences found over the whole trajectory are described in Table 2.

**Table 2. Occurrence of the Most Recurrent Patterns of Hydrogen Bonding Characterized by the Number of Bonds Given to Silanol and Water and Received from Silanol and Water<sup>a</sup>**

pattern	occurrence (%)	donating to silanol	accepting from silanol	donating to water	accepting from water
1	22.4	0	0	2	2
2	14.9	1	2	1	0
3	9.3	2	1	0	1
4	7.8	0	0	2	1
5	7.3	1	1	1	1
6	6.3	1	1	1	0

<sup>a</sup>Percentages are given with respect to the total number of water molecules.

The six patterns highlighted by this analysis can be divided in two groups: (i) water molecules that do not form any hydrogen bond with a silanol group (patterns 1 and 4), that can have either four hydrogen bonds (tetragonal arrangement) or three H bonds, similar to bulk water; and (ii) molecules whose adsorption on the inner surface of the nanotube involves at least one hydrogen bond (types 2, 3, 5, and 6). It is worth noting that the mean number of hydrogen bonds for a water molecule not bonded to the surface is 3.65, slightly higher than the bulk value for fSPC water (3.60 hydrogen bonds per water molecule). The most common patterns are represented in Figure 9. For adsorbed molecules, the most common pattern is an "upright" water molecule (pattern 2, Figure 9b), in a plane bisecting the triangular adsorption site. This water molecule receives two H bonds from two silanol groups and donates one

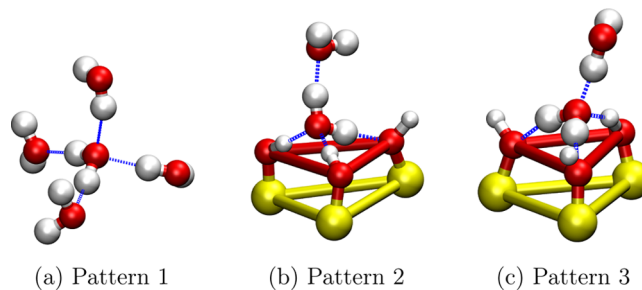


**Figure 9.** Illustration of the most common hydrogen bonding patterns for water in an imogolite nanotube. For the numbering of patterns, see Table 2.

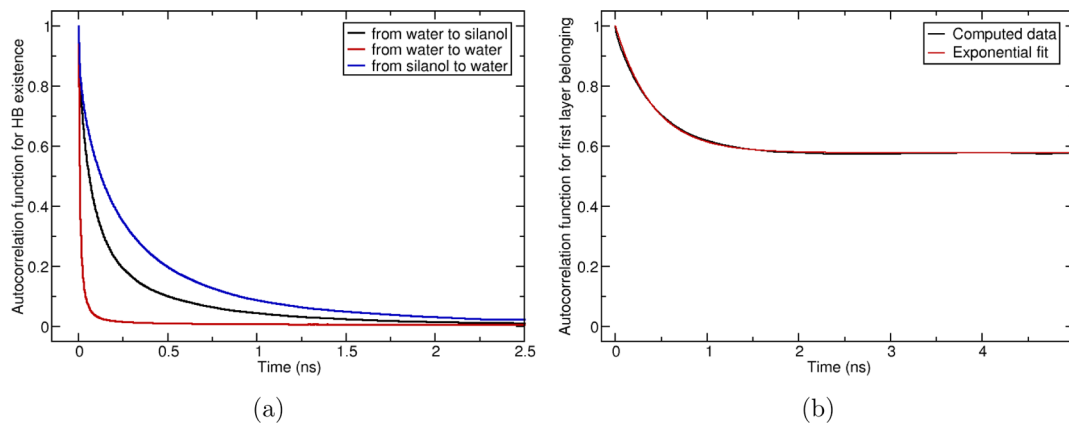


**Figure 10.** (a) Autocorrelation of the hydrogen bond existence for three types of donor–acceptor couples: water–silanol (black line), silanol–water (blue line), and water–water (red line). (b) Autocorrelation of the presence in the first adsorbed layer. The computed data (black line) were fitted by an exponential function (red line),  $y = 1 + 0.42 \left( \exp\left(-\frac{x}{0.41}\right) - 1 \right)$ .

hydrogen bond to the third silanol. A water hydroxyl group is left pointing toward the center of the nanotube, free to donate a hydrogen bond to a water molecule of the second layer. This creates a structuration of the adsorbed water beyond the first layer, which is clearly visible in the density maps (Figures 4 and 5), with a favorable position for water oxygen atoms across that pending hydroxyl group. It also defines an equilibrium distance between the first and second layer of adsorption, which corresponds to a water–water hydrogen bond length.

The second most common pattern for the first layer of water is a water molecule lying “flat” on the inner imogolite surface, donating two H bonds to neighboring silanol groups and receiving one from the third silanol neighbor. This allows the formation of a fourth hydrogen bond from a water molecule outside of the first layer. In this case, the direction of the hydrogen bond is less constrained, explaining the “diffuse” part of the oxygen density in the second water layer, as seen in Figure 5.

Large possibilities of organization of the first layer of adsorbed water molecules, with orientational disorder, are reminiscent of the theory of Bernal and Fowler,<sup>35</sup> regarding ice rules. From the energetics of each individual configurations, as well as the frustration arising from constraints (no more than two H bonds can be donated or received, and no two neighboring adsorption sites can be populated at the same time), we believe that a model of the orientational disorder in that strongly bound layer of adsorbed water could be constructed, possibly explaining why the adsorption sites are only occupied at nearly 38% at saturation uptake.

**Water Dynamics.** From the structural analysis of the water density and the hydrogen bonds in the adsorbed water, there are clear hints at the dynamic nature of the system and the lability of the water molecules. We have seen that hydrogen bond patterns are statistically distributed among several configurations, and that there is anisotropic surface diffusion in the first layer of adsorbed water (see Figure 7 and accompanying text). Analysis of trajectories shows that this surface diffusion occurs without breaking all of the hydrogen bonds involved. By breaking a single hydrogen bond, an adsorbed water molecule can flip around the axis formed by the remaining silanol groups and thereby diffuses to the adjacent site, then reforms a hydrogen bond with another SiOH group. Because the triangular sites are isosceles and the surface is curved, the flip is easier and requires less configurational change

within the furrows than crossing the silicon rings. This explains the preferential circular diffusion as opposed to the axial diffusion in fully loaded nanotube. In this section, we go further to quantify the dynamics of the water inside the imogolite nanotube.

To do so, we calculated autocorrelation functions of the presence of water molecules, both within the first adsorption layer and in the less-ordered “core” of the tube. Because of the relatively slow dynamics of the strongly confined water, these quantities were calculated from 50 ns classical trajectories. For all three possible donor–acceptor hydrogen bond types, we computed autocorrelation functions that are plotted in Figure 10a. From these autocorrelation functions, the lifetime of each H bond type was extracted and are presented in Table 3. The autocorrelation decay is not strictly exponential because the hydrogen bonds form multiple populations (first and second layer, etc.) with different decays.

**Table 3. Characteristic Lifetime for Hydrogen Bonds Calculated from the Time Length for the Autocorrelation Function To Decay to 50%**

donor	acceptor	characteristic time $\tau$ (ps)
water	water	4.43
water	silanol	57.43
silanol	water	123.5

First, looking at the water–water hydrogen bonds, we see that their lifetime is roughly three times higher in the imogolite nanotube than in bulk water (calculated at 1.68 ps from a simulation of pure fSPC water). This slowdown of the water dynamics under confinement has been well-studied and explained in previous work and is due in part to the stronger organization of the water, and in part to excluded volume effects (a water molecule finding fewer partners to “switch” a hydrogen bond to).<sup>36,37</sup> Second, we see that hydrogen bonds between water and the silanol-rich surface have a lifetime more than an order of magnitude greater than water–water H bonds. A study on hydrogen bonding of water on the  $\alpha$ -quartz interface—whose (001) surface is chemically similar to imogolite, in that it presents geminal silanol groups—calculated persistence times of SiOH–water hydrogen bonds between 160 and 170 fs.<sup>38</sup> The extremely large difference, and the very strong bonding of water on the imogolite inner surface, can be

explained by the cooperative effect of the formation of three hydrogen bonds, on top of which is present the generic confinement slowdown.

We also investigated the residence time of water molecules in the first adsorbed layer, inside the imogolite nanotube. There are two ways to define the “first layer”, by using geometrical radius or by considering molecules that form at least one hydrogen bond with the surface. We chose the latter option, which is more chemically robust. The time autocorrelation function deriving from it is plotted in Figure 10b. It shows an exponential decay and reaches a plateau at 57%, that is, the average percentage of water molecules that belong to that first layer. The decay time for the autocorrelation function is found to be 410 ps. This is two or four times larger than the indicative lifetimes of hydrogen bonds with the surface (donated or received by the silanol group, respectively). This confirms the existence of an “inner surface diffusion” mechanism that allows diffusion between adsorption sites without exiting the layer itself. We can also compare this lifetime to residence times in protein adsorption sites. For example, for myoglobin,<sup>39</sup> residence times span from 10 to 450 ps, where the unusually high residence times (>80 ps) correspond to water trapped either in the cavities inside the protein or in the grooves and concave regions.

To complete this study, we extracted diffusion coefficients from mean-square displacement (Figure S4) of water molecules in the nanotube. We find a diffusion coefficient in the *z*-axis of  $3.5 \times 10^{-6}$  cm<sup>2</sup>/s, which is three times smaller than the coefficient calculated by Zang et al.<sup>40</sup> for a similar but lower water density. Moreover, we do not see a long-time diffusive behavior in the *xy* plane because of the confinement.

## CONCLUSIONS AND PERSPECTIVES

This study of the properties of water adsorbed inside hydrophilic imogolite nanotubes was motivated by the understanding of the specific behavior of water because of its tight confinement, with numerous silanol groups on the inner surface of the nanotubes. Because of the strong interactions between water and imogolite and the slow dynamics of the confined water, we relied on a classical force field to perform MD studies. We validated the CLAYFF force field and found that it had to be employed in its extended version—with a Si—O—H bending term—to correctly reproduce the reference data we had produced from first-principles MD. This is in contrast with conventional clay materials, where this term is not as important, and is ascribed to the strong curvature of the imogolite surface.

We then developed a model for the structure of adsorbed water, based on the calculated atomic densities and statistical analysis of the hydrogen bonding patterns observed between water molecules and silanol groups. We show that adsorption in the first layer vicinal to the imogolite tube can be described by an anisotropic triangular lattice of adsorption sites, which are not fully populated. We showed that interactions between the water molecules adsorbed at neighboring sites are complex, based on (i) exclusion of some nearest neighbor pairs (where the sites are too close to be occupied at the same time) and (ii) the number of hydrogen bonds donated (and accepted) by the water molecules to (and from) neighboring silanol groups. Maximizing the number of hydrogen bonds created, while adhering to these rules, creates frustration in the system and leads to the emergence of a heavily disordered state. This situation is very similar to the Bernal–Fowler rules describing

the orientation of water molecules in ice.<sup>35</sup> Finally, we also characterized the dynamics of the confined water molecules, as well as the hydrogen bonds. We find that in addition to the generic effect of the slowdown of confined water, the strong interactions of water molecules with the silanol groups giving rise to lifetimes that compare to typical residence times of water in protein adsorption sites.

In the future, it would be interesting to extend this study of the structure of adsorbed water at varying temperature or with changes in the imogolite nanotube size (from the value of *n* = 12 repeating units used in this study). Another noteworthy perspective would be to consider the possibility of partial or total functionalization of the silanol groups—replacing, for example, some of the hydrophilic—SiOH groups with hydrophobic—SiOCH<sub>3</sub>. This would affect the overall affinity of the internal surface of the imogolite nanotubes for water, tuning them from very hydrophilic to potentially hydrophobic,<sup>41</sup> and changing the thermodynamics of adsorption. It would also introduce more frustration into the adsorbed water and change the “ice rules”, affecting the structure of the confined phase. This could be studied by atomistic simulations, as was performed here, or at a more fundamental scale by an Ising-type model of the adsorbed water molecules, dictated by the energies of the various possible configurations of neighboring water molecules and silanol groups.

## ASSOCIATED CONTENT

### S Supporting Information

The Supporting Information is available free of charge on the ACS Publications website at DOI: [10.1021/acs.langmuir.8b01115](https://doi.org/10.1021/acs.langmuir.8b01115).

GCMC adsorption models, adsorption isotherms, additional structural information, and mean-square displacement of adsorbed water ([PDF](#))

## AUTHOR INFORMATION

### Corresponding Authors

\*E-mail: anne.boutin@ens.fr (A.B.).

\*E-mail: fx.coudert@chimie-paristech.fr (F.-X.C.).

### ORCID

Anne Boutin: [0000-0003-4209-1652](#)

François-Xavier Coudert: [0000-0001-5318-3910](#)

### Notes

The authors declare no competing financial interest.

## ACKNOWLEDGMENTS

We thank Antoine Thill, Sophie Le Caer, and Yuanyuan Liao for the fruitful discussions. We acknowledge access to the CINES high-performance computing platforms provided by a GENCI grant (A0030807069).

## REFERENCES

- (1) Yoshinaga, N.; Aomine, S. Imogolite in some ando soils. *Soil Sci. Plant Nutr.* **1962**, *8*, 22–29.
- (2) Amara, M.-S.; Paineau, E.; Bacia-Verloop, M.; Krapf, M.-E. M.; Davidson, P.; Belloni, L.; Levard, C.; Rose, J.; Launois, P.; Thill, A. Single-step formation of micron long (OH)<sub>3</sub>Al<sub>2</sub>O<sub>3</sub>Ge(OH) imogolite-like nanotubes. *Chem. Commun.* **2013**, *49*, 11284.
- (3) Gustafsson, J. P. The Surface Chemistry of Imogolite. *Clays Clay Miner.* **2001**, *49*, 73–80.

- (4) Guimarães, L.; Enyashin, A. N.; Frenzel, J.; Heine, T.; Duarte, H. A.; Seifert, G. Imogolite Nanotubes: Stability, Electronic, and Mechanical Properties. *ACS Nano* **2007**, *1*, 362–368.
- (5) Tamura, K.; Kawamura, K. Molecular Dynamics Modeling of Tubular Aluminum Silicate: Imogolite. *J. Phys. Chem. B* **2002**, *106*, 271–278.
- (6) Zhao, M.; Xia, Y.; Mei, L. Energetic Minimum Structures of Imogolite Nanotubes: A First-Principles Prediction. *J. Phys. Chem. C* **2009**, *113*, 14834–14837.
- (7) Demichelis, R.; Noël, Y.; D'Arco, P.; Maschio, L.; Orlando, R.; Dovesi, R. Structure and energetics of imogolite: a quantum mechanical ab initio study with B3LYP hybrid functional. *J. Mater. Chem.* **2010**, *20*, 10417.
- (8) Alvarez-Ramírez, F. *Ab initio* simulation of the structural and electronic properties of aluminosilicate and aluminogermanate nanotubes with imogolite-like structure. *Phys. Rev. B: Condens. Matter Mater. Phys.* **2007**, *76*, 125421.
- (9) Konduri, S.; Mukherjee, S.; Nair, S. Controlling Nanotube Dimensions: Correlation between Composition, Diameter, and Internal Energy of Single-Walled Mixed Oxide Nanotubes. *ACS Nano* **2007**, *1*, 393–402.
- (10) Lee, S. U.; Choi, Y. C.; Youm, S. G.; Sohn, D. Origin of the Strain Energy Minimum in Imogolite Nanotubes. *J. Phys. Chem. C* **2011**, *115*, 5226–5231.
- (11) González, R. I.; Ramírez, R.; Rogan, J.; Valdivia, J. A.; Munoz, F.; Valencia, F.; Ramírez, M.; Kiwi, M. Model for Self-Rolling of an Aluminosilicate Sheet into a Single-Walled Imogolite Nanotube. *J. Phys. Chem. C* **2014**, *118*, 28227–28233.
- (12) González, R. I.; Rogan, J.; Bringa, E. M.; Valdivia, J. A. Mechanical Response of Aluminosilicate Nanotubes under Compression. *J. Phys. Chem. C* **2016**, *120*, 14428–14434.
- (13) Amara, M. S.; Rouzière, S.; Paineau, E.; Bacia-Verloop, M.; Thill, A.; Launois, P. Hexagonalization of Aluminogermanate Imogolite Nanotubes Organized into Closed-Packed Bundles. *J. Phys. Chem. C* **2014**, *118*, 9299–9306.
- (14) Creton, B.; Bougeard, D.; Smirnov, K. S.; Guilment, J.; Poncelet, O. Molecular dynamics study of hydrated imogolite : 2. Structure and dynamics of confined water. *Phys. Chem. Chem. Phys.* **2008**, *10*, 4879.
- (15) Cradwick, P. D. G.; Farmer, V. C.; Russell, J. D.; Masson, C. R.; Wada, K.; Yoshinaga, N. Imogolite, a Hydrated Aluminium Silicate of Tubular Structure. *Nature, Phys. Sci.* **1972**, *240*, 187–189.
- (16) Aroyo, M. I.; Perez-Mato, J. M.; Capillas, C.; Kroumova, E.; Ivantchev, S.; Madariaga, G.; Kirov, A.; Wondratschek, H. Bilbao Crystallographic Server: I. Databases and crystallographic computing programs. *Z. Kristallogr.—Cryst. Mater.* **2006**, *221*, 15–27.
- (17) Konduri, S.; Tong, H. M.; Chempath, S.; Nair, S. Water in Single-Walled Aluminosilicate Nanotubes: Diffusion and Adsorption Properties. *J. Phys. Chem. C* **2008**, *112*, 15367–15374.
- (18) Ackerman, W. C.; Smith, D. M.; Huling, J. C.; Kim, Y. W.; Bailey, J. K.; Brinker, C. J. Gas/vapor adsorption in imogolite: a microporous tubular aluminosilicate. *Langmuir* **1993**, *9*, 1051–1057.
- (19) Mukherjee, S.; Bartlow, V. M.; Nair, S. Phenomenology of the Growth of Single-Walled Aluminosilicate and Aluminogermanate Nanotubes of Precise Dimensions. *Chem. Mater.* **2005**, *17*, 4900–4909.
- (20) Zang, J.; Chempath, S.; Konduri, S.; Nair, S.; Sholl, D. S. Flexibility of Ordered Surface Hydroxyls Influences the Adsorption of Molecules in Single-Walled Aluminosilicate Nanotubes. *J. Phys. Chem. Lett.* **2010**, *1*, 1235–1240.
- (21) Dovesi, R.; Orlando, R.; Erba, A.; Zicovich-Wilson, C. M.; Civalleri, B.; Casassa, S.; Maschio, L.; Ferrabone, M.; De La Pierre, M.; D'Arco, P.; Noël, Y.; Causà, M.; Réat, M.; Kirtman, B. CRYSTAL14: A program for the *ab initio* investigation of crystalline solids. *Int. J. Quantum Chem.* **2014**, *114*, 1287–1317.
- (22) Hutter, J.; Iannuzzi, M.; Schiffmann, F.; VandeVondele, J. CP2K: atomistic simulations of condensed matter systems. *Wiley Interdiscip. Rev.: Comput. Mol. Sci.* **2014**, *4*, 15–25.
- (23) Bussi, G.; Donadio, D.; Parrinello, M. Canonical sampling through velocity rescaling. *J. Chem. Phys.* **2007**, *126*, 014101.
- (24) Plimpton, S. Fast Parallel Algorithms for Short-Range Molecular Dynamics. *J. Comput. Phys.* **1995**, *117*, 1–19.
- (25) Desbiens, N.; Boutin, A.; Demachy, I. Water Condensation in Hydrophobic Silicalite-1 Zeolite: A Molecular Simulation Study. *J. Phys. Chem. B* **2005**, *109*, 24071–24076.
- (26) Cygan, R. T.; Liang, J.-J.; Kalinichev, A. G. Molecular Models of Hydroxide, Oxyhydroxide, and Clay Phases and the Development of a General Force Field. *J. Phys. Chem. B* **2004**, *108*, 1255–1266.
- (27) Teleman, O.; Jönsson, B.; Engström, S. A molecular dynamics simulation of a water model with intramolecular degrees of freedom. *Mol. Phys.* **1987**, *60*, 193–203.
- (28) Pouvreau, M.; Greathouse, J. A.; Cygan, R. T.; Kalinichev, A. G. Structure of Hydrated Gibbsite and Brucite Edge Surfaces: DFT Results and Further Development of the ClayFF Classical Force Field with Metal–O–H Angle Bending Terms. *J. Phys. Chem. C* **2017**, *121*, 14757–14771.
- (29) Coudert, F.-X.; Cailliez, F.; Vuilleumier, R.; Fuchs, A. H.; Boutin, A. Water nanodroplets confined in zeolite pores. *Faraday Discuss.* **2009**, *141*, 377–398.
- (30) Gor, G. Y.; Bernstein, N. Adsorption-Induced Surface Stresses of the Water/Quartz Interface: Ab Initio Molecular Dynamics Study. *Langmuir* **2016**, *32*, 5259–5266.
- (31) Neimark, A. V.; Coudert, F.-X.; Boutin, A.; Fuchs, A. H. Stress-Based Model for the Breathing of Metal–Organic Frameworks. *J. Phys. Chem. Lett.* **2009**, *1*, 445–449.
- (32) Mouhat, F.; Bousquet, D.; Boutin, A.; Bouëssel du Bourg, L.; Coudert, F.-X.; Fuchs, A. H. Softening upon Adsorption in Microporous Materials: A Counterintuitive Mechanical Response. *J. Phys. Chem. Lett.* **2015**, *6*, 4265–4269.
- (33) Haigis, V.; Coudert, F.-X.; Vuilleumier, R.; Boutin, A. Investigation of structure and dynamics of the hydrated metal–organic framework MIL-53(Cr) using first-principles molecular dynamics. *Phys. Chem. Chem. Phys.* **2013**, *15*, 19049.
- (34) Luzar, A.; Chandler, D. Hydrogen-bond kinetics in liquid water. *Nature* **1996**, *379*, 55–57.
- (35) Bernal, J. D.; Fowler, R. H. A Theory of Water and Ionic Solution, with Particular Reference to Hydrogen and Hydroxyl Ions. *J. Chem. Phys.* **1933**, *1*, 515–548.
- (36) Fogarty, A. C.; Coudert, F.-X.; Boutin, A.; Laage, D. Reorientational Dynamics of Water Confined in Zeolites. *Chem-PhysChem* **2014**, *15*, 521–529.
- (37) Fogarty, A. C.; Duboué-Dijon, E.; Laage, D.; Thompson, W. H. Origins of the non-exponential reorientation dynamics of nano-confined water. *J. Chem. Phys.* **2014**, *141*, 18C523.
- (38) Ozkanlar, A.; Kelley, M.; Clark, A. Water Organization and Dynamics on Mineral Surfaces Interrogated by Graph Theoretical Analyses of Intermolecular Chemical Networks. *Minerals* **2014**, *4*, 118–129.
- (39) Makarov, V. A.; Andrews, B. K.; Smith, P. E.; Pettitt, B. M. Residence Times of Water Molecules in the Hydration Sites of Myoglobin. *Biophys. J.* **2000**, *79*, 2966–2974.
- (40) Zang, J.; Konduri, S.; Nair, S.; Sholl, D. S. Self-Diffusion of Water and Simple Alcohols in Single-Walled Aluminosilicate Nanotubes. *ACS Nano* **2009**, *3*, 1548–1556.
- (41) Bonelli, B. *Developments in Clay Science*; Elsevier, 2016; Vol. 7; pp 279–307.